

Pathways, timing, and evolution of Pacific winter water through Barrow Canyon

E. L. Shroyer^{a,*}, Robert S. Pickart^b

^a*Oregon State University*

^b*Woods Hole Oceanographic Institution*

Abstract

Observations from a ship-based campaign in July-August 2009, combined with idealized numerical simulations, are used to investigate the seasonal delivery of Pacific winter water to Barrow Canyon and the subsequent adjustment of the flow down the canyon. As the current advects dense water, it transitions from a nearly barotropic structure near the canyon head to a strongly baroclinic flow with a subsurface maximum near the canyon mouth. Both the data and model indicate that the transit times along the three Chukchi shelf pathways feeding Barrow Canyon – a coastal pathway, a southern Hanna Shoal pathway, and a northern Hanna Shoal pathway – modulate the mode of winter water that occupies the canyon at a given time. In particular, remnant winter water carried along the rapid coastal pathway can precede the arrival of newly ventilated Pacific winter water carried along the two interior pathways. The observations and model indicate that the transition between water types draining from the canyon can occur rapidly over time scales of days to weeks. We also demonstrate that mixing along the path of the current is unlikely to result in the observed down-canyon transition from newly ventilated Pacific winter water to remnant winter water, further supporting the dominant role of advection. While the focus here is on the transition of winter water modes, the implication that seasonality within Barrow Canyon is tied to seasonality of the Bering Strait inflow, together with the relative transit times along advective pathways, should hold for other water types as well.

* *Corresponding author:* Emily Shroyer, Oregon State University, 104 CEOAS Administration Building, Corvallis, OR 97331-5503. Email: eshroyer@coas.oregonstate.edu

Keywords: Chukchi Sea, Barrow Canyon, Beaufort Sea, Pacific winter water, Alaskan Coastal Current

1. Introduction

Barrow Canyon, located in the northeast corner of the Chukchi Sea, is a primary route by which Pacific water exits the Chukchi Sea. As such it represents a critical control point for dictating the fate of this water in the western Arctic Ocean. North of Bering Strait, the flow of Pacific water across the Chukchi shelf is strongly influenced by topography and tends to follow three main pathways (Fig. 1). Barrow Canyon is located at the terminus of the eastern most pathway, which flows adjacent to the Alaskan coast. Some of the water transiting via the other two pathways, to the west through Herald Canyon and within the Central Channel (between Herald and Hanna Shoals, Weingartner et al. (2005)), is routed through Barrow Canyon as well. Observations (e.g., Weingartner, 2012) and model studies (Winsor and Chapman, 2004; Spall, 2007) suggest that Pacific water circulates clockwise around the northern bank of Hanna Shoal, with a portion diverted south of the shoal as well (Pickart et al., 2016, Fig. 1). These alternate routes then meet the coastal pathway near the head of Barrow Canyon and transit down the canyon. To the west of the canyon there is an eastward-flowing shelfbreak jet carrying Pacific water from the western-most pathway in Fig. 1 (Corlett and Pickart, 2017). Thus, Barrow Canyon represents a confluence of numerous branches of Pacific water on the northeastern Chukchi shelf.

At the mouth of the canyon Pacific water exits into the basin via different mechanisms. A portion of the water veers to the east and forms the Beaufort shelfbreak jet (Pickart et al., 2005a; Okkonen et al., 2009), although the transport of the jet only accounts for a small fraction of the Bering Strait inflow (Nikolopoulos et al., 2009; Brugler et al., 2014). Recently it has been documented that a substantial amount of the Pacific water turns to the west as it exits the canyon and forms a current over the Chukchi continental slope (Corlett and Pickart, 2017). Using a collection of shipboard transects occupied over more than a decade, Corlett and Pickart (2017) determined that the current is present in all wind conditions and

26 transports $O(0.5 \text{ Sv})$ of Pacific water westward. Mooring data have documented that the
27 current, known as the Chukchi slope current, is present year-round (Li and Pickart, 2017).
28 Pacific water can also exit Barrow Canyon via turbulent processes. The structure of the
29 flow in the canyon satisfies the necessary conditions for baroclinic instability (Pickart et al.,
30 2005a), and anti-cyclonic eddies (Pickart and Stossmeister, 2008) and filaments of Pacific
31 water (Okkonen et al., 2009; Brugler et al., 2014) have been observed emanating from the
32 canyon.

33 Water mass properties within the Chukchi Sea are set by advection through the Bering
34 Strait in combination with local modification via air-ice-sea interaction, including ice forma-
35 tion and melt, and diapycnal mixing. In summer and early fall, the western side of Bering
36 Strait typically contains nutrient- and carbon-rich Anadyr water, which has origins that
37 extend to the Gulf of Anadyr in the northwest Bering Sea (Coachman et al., 1975). North
38 of the strait this water mixes with Bering shelf water, derived from the central Bering Sea
39 and northern Bering shelf, to form a water mass known as Bering summer water. (This
40 water mass has also been called summer Bering Sea water, western Chukchi summer water,
41 and Chukchi summer water.) During this time of year the eastern channel of the strait
42 contains warm and fresh Alaskan coastal water, which is advected by the Alaskan Coastal
43 Current (ACC). Progressing northward, the Bering summer water is found predominantly in
44 the western and central pathways, while the Alaskan coastal water is confined to the ACC.
45 However, wind forcing can cause these two summer water masses to penetrate into different
46 regions of the Chukchi shelf (Weingartner et al., 2005; Pisareva et al., 2015).

47 In winter and early-spring, a well-defined (in temperature and salinity space) water mass
48 with temperatures near the freezing point flows through Bering Strait (Aagaard and Roach,
49 1990; Weingartner et al., 1998; Woodgate and Aagaard, 2005). We refer to this water mass
50 as newly ventilated Pacific winter water (PWW), which is taken to be $< -1.65^\circ\text{C}$. PWW
51 is formed in the northern Bering Sea (Muench et al., 1988) and can be further transformed
52 on the Chukchi shelf within large polynyas (Weingartner et al., 1998; Itoh et al., 2012) and
53 within smaller leads and openings (Pacini et al., this issue). If the transformation is extensive

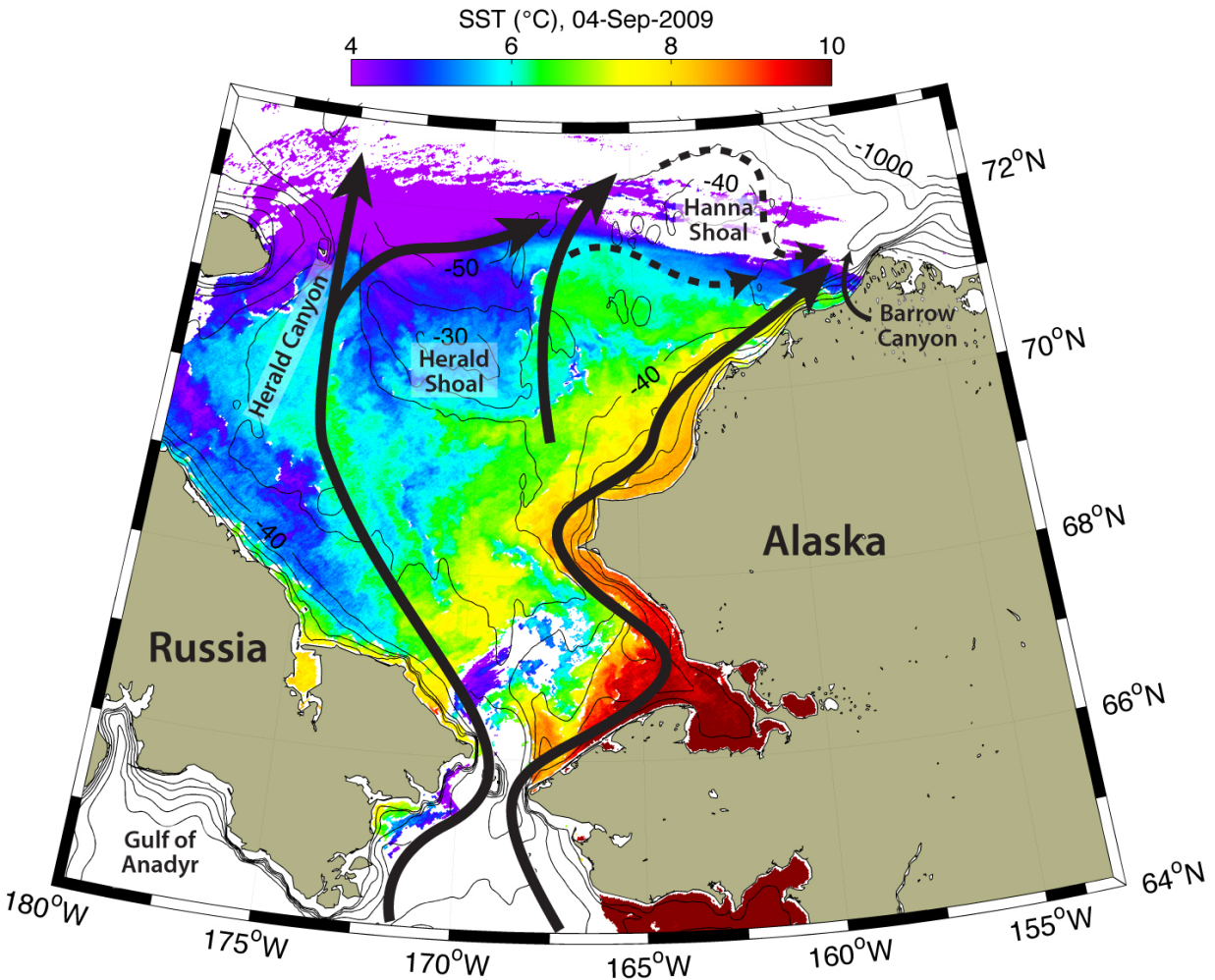


Figure 1: Modis SST image for the Chukchi Sea taken on 4 September 2009, approximately one month after the shipboard survey was completed. This image highlights circulation paths within the Chukchi Sea, which are schematically indicated by arrows (and consistent with previous circulation diagrams, e.g. Gong and Pickart, 2015). The dashed arrows near the northeast corner indicate circulation around Hanna Shoal.

54 enough, the water is classified as “hypersaline” winter water. This salty and dense variety
 55 of winter water is at times observed flowing northward through Barrow Canyon (Itoh et al.,
 56 2012), and it can also be upwelled from the basin into the canyon (Pisareva et al., this
 57 issue). After winter, PWW is modified by mixing and/or atmospheric warming (e.g., Gong
 58 and Pickart, 2015). We refer to this modified product as remnant winter water (RWW),
 59 which is taken to be in the temperature range -1 to -1.65°C. This water comprises the bulk

60 of the upper portion of the cold halocline throughout the western Arctic Ocean (Steele et al.,
61 2004).

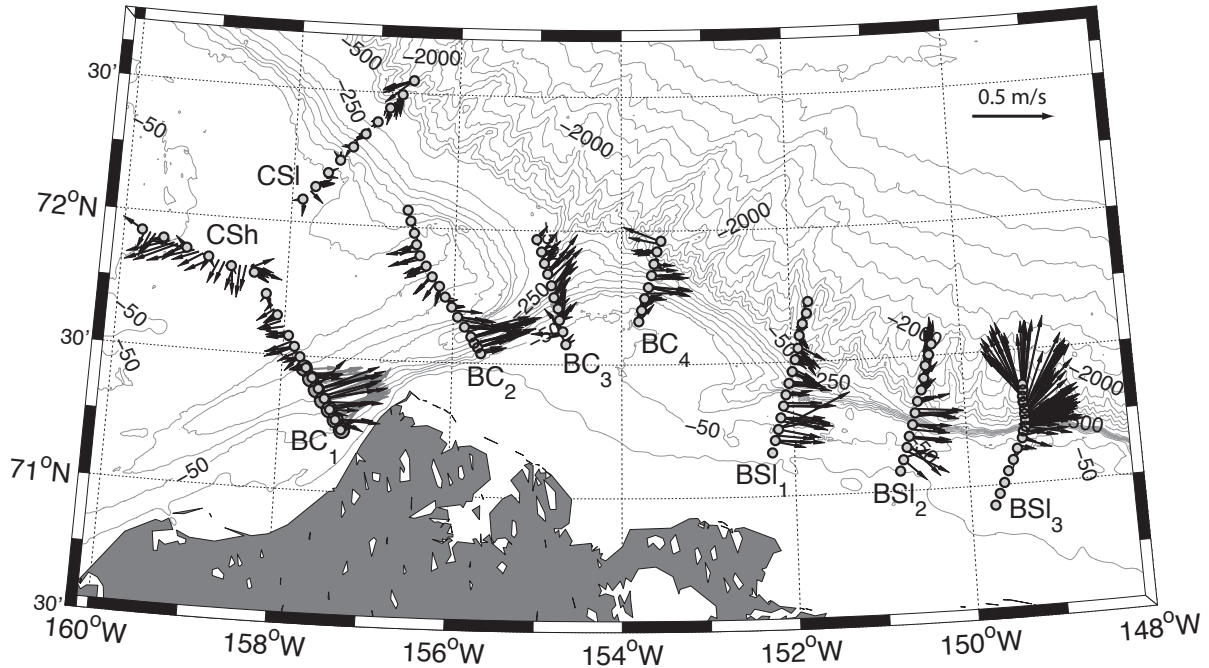


Figure 2: Map of the observational study area showing the locations of the CTD profiles occupied during the cruise (open circles). Hydrographic/velocity transects were made over the Chukchi Shelf (*CSh*), across the Chukchi Slope (*CSl*), within Barrow Canyon (*BC*), and across the Beaufort Slope (*BSl*). The vectors denote the depth mean (to a maximum of roughly 250 m) velocity from the vessel-mounted acoustic Doppler current profiler. The *BC*₁ transect was occupied twice (dark and light grey circles, grey and black vectors), near the beginning and end of the cruise.

62 Spatial and temporal variability in both inflow and water mass composition at Bering
63 Strait, combined with a large range in residence times within the Chukchi Sea (from a few
64 months to a year according to Spall (2007)), create the potential for storage, modification,
65 and mixing of various Pacific water masses within the Chukchi Sea. This is particularly
66 true in Barrow Canyon where the multiple pathways reunite. As such, it is common for
67 winter and summer water masses to co-exist within the canyon (e.g., Pickart et al., 2005b;
68 Shroyer, 2012; Pickart et al., this issue). For example, Pickart et al. (2005b) examined two

69 sections occupied across the canyon during a time when both the ACC was present as well
 70 as a deeper flow of PWW. They observed that the layer of PWW adjusted via deceleration
 71 and stretching as it descended down-canyon; their analysis also indicated that hydraulic
 72 control and/or mixing may be important processes within Barrow Canyon. However, the
 73 data coverage in that survey did not extend beyond the middle of the canyon.

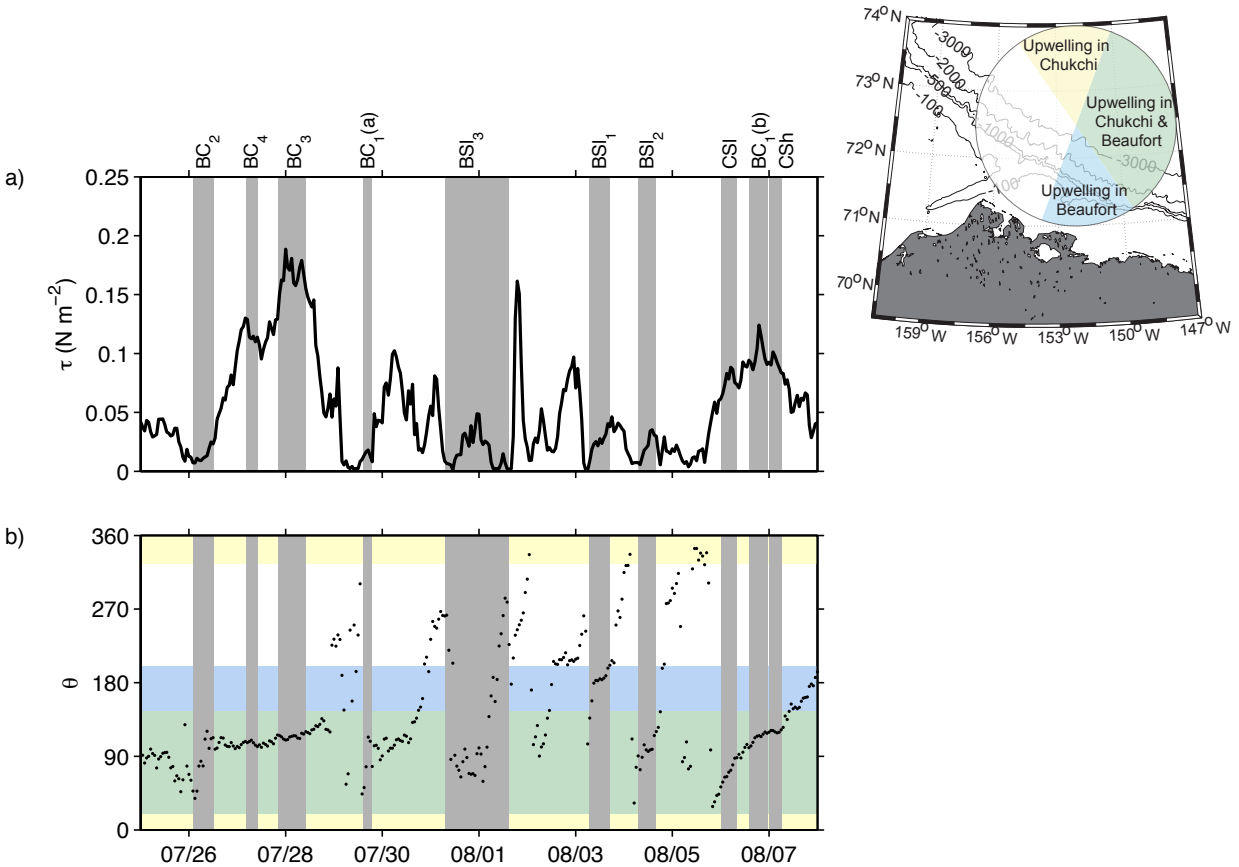


Figure 3: a) Wind stress and b) direction (from which the winds are blowing) during the cruise using the Pt. Barrow weather station data. The time periods of the CTD transect lines are shaded in grey and labeled at the top. Colored bands in the bottom panel denote approximate regions of upwelling favorable winds for the Beaufort shelf (blue), Chukchi shelf (yellow), and both shelves (green), as defined within the map inset.

74 Both the seasonality and synoptic variability of the circulation in Barrow Canyon is
 75 largely attributable to the winds (Weingartner et al., 1998; Okkonen et al., 2009). The
 76 prevailing winds are northeasterly and tend to retard the mean flow. During summer, when

77 the winds are weakest, the northward transport through the canyon is maximum (Itoh et al.,
78 2012; Weingartner et al., in press). Based on a 36-year wind-transport hindcast at the head
79 of the canyon, Weingartner et al. (in press) argues that there is weak southward transport
80 during the fall and near-zero transport during winter. On shorter timescales, upwelling
81 favorable winds arise due to the influence of both the Beaufort High and Aleutian Low
82 (Weingartner et al., in press; Pisareva et al., this issue; Pickart et al., this issue). Using two
83 years of mooring data near the head of the canyon, Pisareva et al. (this issue) found that
84 the most common water mass upwelled from the basin was cold winter water (both PWW
85 and RWW). At times, however, the winds drive Atlantic water from the lower halocline into
86 the canyon (e.g., Mountain et al., 1976; Münchow and Carmack, 1997; Weingartner et al.,
87 1998). The upwelling of Atlantic water occurs most often during the late fall to early spring
88 (Pisareva et al., this issue), likely because the Pacific-Atlantic water interface seaward of
89 the canyon is shallower at this time of year, making the Atlantic water more accessible (Lin
90 et al., this issue). Occasionally, Atlantic Water intrudes far onto the Chukchi shelf (Bourke
91 and Paquette, 1976; Ladd et al., 2016).

92 The motivation for the present study is to enhance our knowledge of the timing of winter
93 water delivery to Barrow Canyon and the subsequent adjustment of the flow down the
94 canyon. The ultimate aim is to better understand how this complex choke point influences
95 the fate of Pacific water. We focus on the evolution and dynamics of the winter water
96 (PWW and RWW) as it approaches and exits the canyon under weak atmospheric forcing
97 in summer. We use data from a 2009 hydrographic/velocity survey that captured dense
98 PWW descending down Barrow Canyon, transitioning from a nearly barotropic structure
99 to one with pronounced baroclinicity characterized by a sub-surface current maximum. To
100 complement the data analysis, we use a simplified numerical model to investigate the transit
101 times in the Chukchi Sea and the arrival of various water masses within Barrow Canyon.
102 The measurements are detailed in Section 2. An overview of the wind field and component
103 water masses is presented in Section 3. The observational analysis appears in Section 4, and
104 a comparison with the results of the model is presented in Section 5.

105 2. Measurements

106 From 26 July – 7 August 2009, ten hydrographic/velocity sections were occupied in the
107 vicinity of the shelf edge in the eastern Chukchi and western Beaufort Seas from the USCGC
108 *Healy*. Locations of the Conductivity-Temperature-Depth (CTD) profiles are shown in Fig-
109 ure 2. The station spacing was sufficient to resolve the internal deformation radius which
110 is less than 10 km in this region. The transects are labeled according to their geographic
111 location as follows: Chukchi Shelf (*CSh*), Chukchi Slope (*CSl*), Barrow Canyon (*BC*), and
112 Beaufort Slope (*BSl*). Numerical subscripts of the sections increase moving downstream
113 (i.e., in the direction of propagation of coastally trapped waves). Transect BC_1 was sampled
114 twice, once near the beginning of the survey (large dark grey circles) and once near the end
115 of the cruise (small light grey circles). Two transects were occupied to the west of Barrow
116 Canyon. Transect *CSh* was the extension of the $BC_1(b)$ transect, positioned between the
117 offshore flank of Barrow Canyon and Hanna Shoal, and transect *CSl* was occupied across
118 the Chukchi slope. Three transects were made to the east of Barrow Canyon across the
119 Beaufort slope ($BSl_{1,2,3}$).

120 The *Healy* was equipped with a Sea-Bird Electronics SBE *9plus* CTD with dual temper-
121 ature and conductivity sensors. Based on laboratory calibration, the temperature accuracy
122 is estimated to be 0.001°C , and, based on calibration with in-situ water samples, the salin-
123 ity is deemed accurate to 0.008 on the shelf and 0.002 in deep water. The CTD downcast
124 data were averaged into 1-m bins that were then used to calculate potential temperature
125 (hereafter referred to simply as temperature), potential density (referred to as density), and
126 buoyancy frequency (N^2).

127 Velocity data were collected using a vessel-mounted RD Instruments (RDI) 75 KHz
128 Acoustic Doppler Current Profiler (ADCP), configured to obtain 5-minute averaged pro-
129 files with a vertical bin size of 8 m. The data were acquired using the VMDAS software, and
130 were processed post-cruise using the the University of Hawaii software package CODAS. Data
131 were flagged for outliers using standard RDI metrics (percent good and backscatter). The
132 barotropic tidal signal was removed from the velocity profiles using the Oregon State Uni-

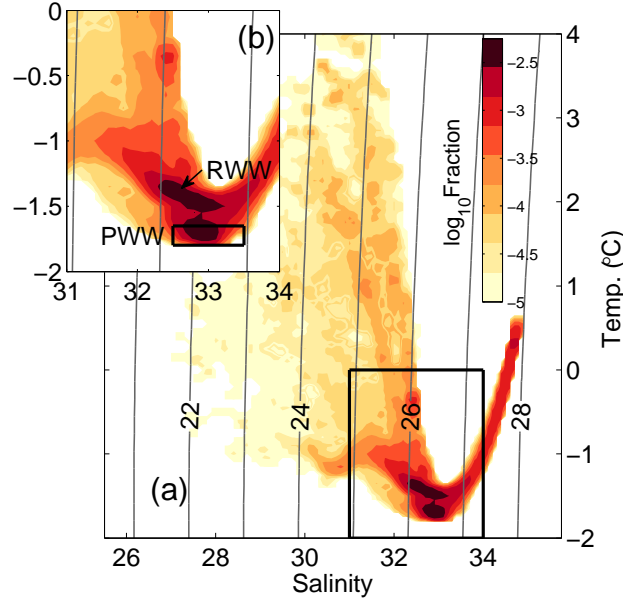


Figure 4: a) TS-histogram plot for depths shallower than 250 m from all sections. b) Enlarged view highlighting the bimodal structure of the Pacific winter water. PWW = newly ventilated winter water; RWW = remnant winter water.

133 versity barotropic tidal prediction model (Padman and Erofeeva, 2004). The profiles along
 134 each transect were then rotated into along- and across-stream components by minimizing
 135 the magnitude of the vertically averaged cross-stream velocity.

136 Turbulent kinetic energy (TKE) dissipation, ϵ (W kg^{-1}), was estimated from Thorpe
 137 overturns calculated from 10-cm averages of density (Thorpe, 1977). Processing of Thorpe
 138 overturns (L_T) followed Galbraith and Kelley (1996), and L_T smaller than that resolvable
 139 given sampling constraints were discarded. Two limiting values were used. The first, 0.5
 140 m ($5\delta z$), is related to the vertical sampling; and the second, $(2\frac{\delta\rho}{\delta\rho_0/\delta z})$, where $\delta\rho_0/\delta z$ is the
 141 mean (sorted) density gradient through the overturn, depends on the density resolution of
 142 the sensor ($\delta\rho \sim 0.001 \text{ kg m}^3$). In addition, a run length criterion was imposed in which the
 143 length of points within an overturn was required to exceed that likely to occur for random
 144 noise (Galbraith and Kelley, 1996). Dissipation was calculated using $\epsilon = L_O^2 N^3$ where
 145 $L_O \sim 0.8L_T$ is the Ozmidov scale (Dillon, 1982).

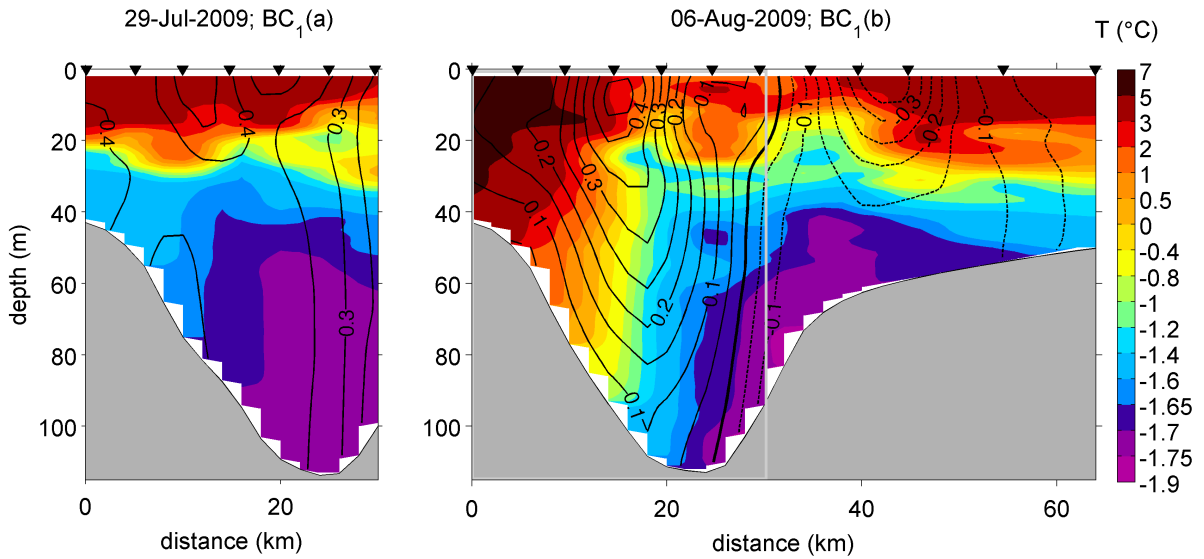


Figure 5: Temperature (color) and velocity (m s^{-1} , contours) for the two upper canyon transects, a) BC_1 (a) and b) BC_1 (b). Note that the temperature color scale is nonlinear and designed to highlight PWW (dark blue-purple). The grey line in BC_1 (b) denotes the geographical extent of BC_1 (a).

146 3. Observational Context

147 At the time of the survey, a well-defined coastal current transported water out of the
 148 Chukchi Sea through Barrow Canyon and continued along the Beaufort slope (Fig. 2).
 149 Ideally, these sections would constitute a synoptic realization. In order to assess this po-
 150 tential, we first consider the wind forcing during the cruise, as well as upstream influences
 151 (e.g., advection of different water masses or shelf wave propagation). The former can be
 152 evaluated using the meteorological data measured at the Pt. Barrow, Alaska Observatory
 153 ([/www.esrl.noaa.gov/gmd/obop/brw](http://www.esrl.noaa.gov/gmd/obop/brw)). With regard to the latter, examination of temper-
 154 ature/salinity (TS) properties provides some guidance as to the importance of upstream
 155 advection, at least in terms of transport of heat and salt. Before analyzing the circulation
 156 and water mass evolution using the shipboard data, we first document the local wind forcing
 157 and overall TS properties measured during the survey.

158 *3.1. Winds*

159 Although variable during the survey period, winds were of moderate amplitude (Fig. 3a)
160 and predominantly directed from the northeast-east (Fig. 3b). This direction corresponds
161 to generally upwelling-favorable conditions for Barrow Canyon and the Beaufort slope. In-
162 dividual wind events typically lasted a few days. Previous analysis of data from the Pt.
163 Barrow Observatory suggest that such moderate wind events are typical this time of year
164 (Shroyer and Plueddemann, 2012), while strong summertime upwelling events are uncom-
165 mon (Pisareva et al., this issue). Based on oceanographic mooring data, flow reversals in
166 Barrow Canyon tend to occur once the upcanyon component of the wind exceeds $5 - 6 \text{ m s}^{-1}$
167 (Weingartner et al., 1998; Pisareva et al., this issue). While Fig. 3 suggests that several of
168 the canyon sections were subject to upwelling favorable winds, the along-canyon wind com-
169 ponent did not exceed 5 m s^{-1} during the any of the canyon transects. For the Beaufort
170 slope, the shelfbreak jet tends to reverse for along-coast winds exceeding 4 m s^{-1} (although
171 this is not always the case, Schulze and Pickart (2012)). The only transect where this con-
172 dition was met was BC_4 (just beyond the mouth of Barrow Canyon). However, the winds
173 ramped up very quickly prior to the occupation of the section, and the current likely did not
174 have time to respond. As shown below, flow reversals along the winter water pathway were
175 not observed in any of the sections, and the associated current transports were consistent
176 with one another throughout the survey. As such, we assume that the survey captured a
177 primarily unforced state of the boundary current system.

178 *3.2. Water Mass Properties*

179 The TS distribution for depths less than 250 m is shown in Figure 4. Cold and relatively
180 fresh TS values (lower left portion of 4a) are likely a mixed-meltwater product. Warm,
181 fresh values (upper left corner of Fig. 4a) are consistent with the properties of Alaskan
182 coastal water. Volumetrically, the contribution from Alaskan coastal water was small; only
183 the second occupation of BC_1 showed the presence of this water mass. Accordingly, this
184 transect is not considered synoptic with the remaining sections. Inclusion of all depths in
185 the TS histogram (not shown) indicates that roughly 50% of the observations are confined

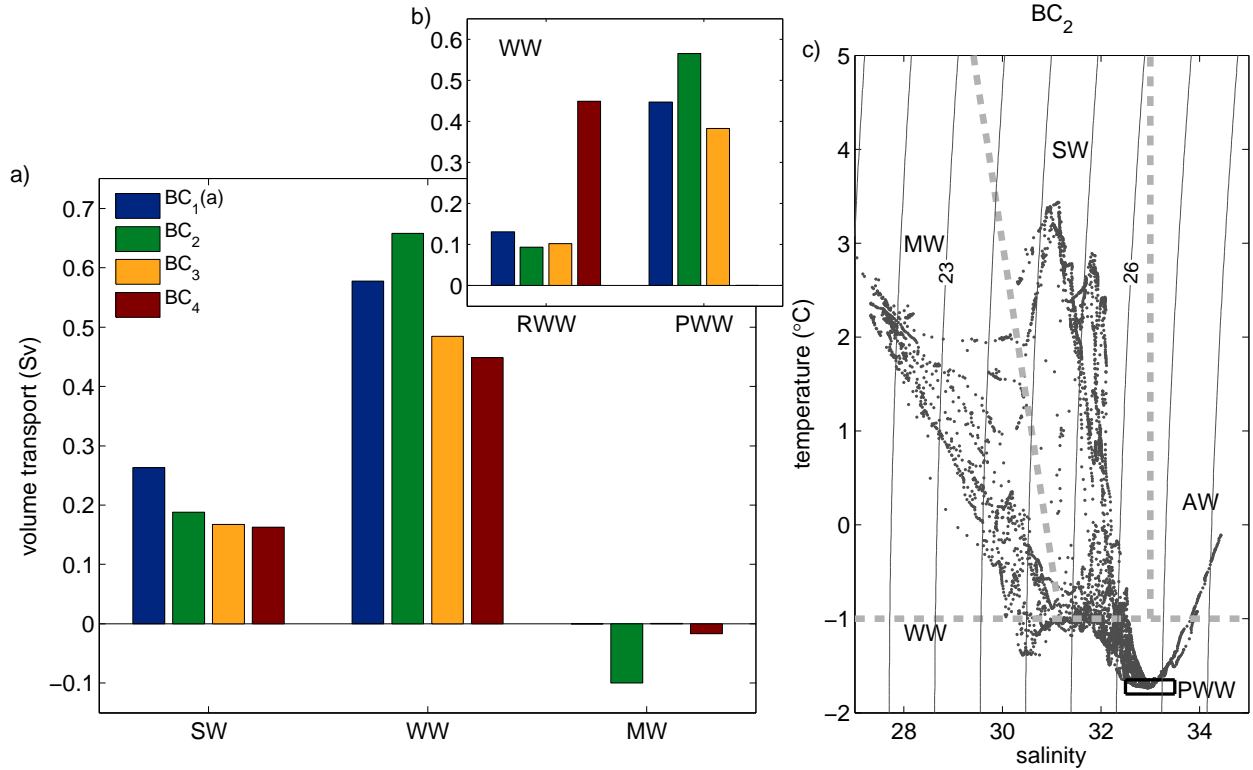


Figure 6: a) Volume transport by TS class for the four CTD sections in Barrow Canyon: $BC_1(a)$, BC_2 , BC_3 , and BC_4 . b) Inset showing the division of Pacific winter water (WW) into newly ventilated winter water (PWW) and remnant winter water (RWW). c) TS plot for the BC_2 transect showing the water mass classes defined in the text: summer water (SW), modified meltwater (MW), Atlantic water (AW), and WW (the PWW subclass is denoted by the box).

186 within a TS-mode near $0.5\text{ }^\circ\text{C}$ and 35, characteristic of Atlantic water that is prevalent in
 187 the deep portion of the sections across the Chukchi and Beaufort slopes.

188 The bulk of the TS measurements above 250 m were associated with the cold and mod-
 189 erately salty winter water that was present during the hydrographic survey (highlighted in
 190 Fig. 4b). Two distinct cold TS-modes were sampled: a lower peak representing PWW and
 191 an upper peak encompassing RWW. Transects $BC_{(1-3)}$, CSh , and CSl , with geographical
 192 ties to the Chukchi Sea, contributed the most to the PWW peak. In contrast, the coldest
 193 waters observed in sections $BSl_{(1-3)}$ and BC_4 were slightly warmer and located in the upper
 194 RWW mode. This geographical distribution of the two types of winter water is suggestive

195 of at least two possibilities. The first interpretation is that PWW is transformed via mixing
196 into RWW along the path of the current as it emanates from the canyon, and that our
197 survey encompassed the segment of the current over which this modification takes place.
198 The second possibility is that, at the time of the survey, PWW was just beginning to flow
199 through the canyon. The latter interpretation is consistent with the results of Pickart et al.
200 (this issue) who deduced that PWW is delivered to the canyon at this time of year via the
201 slower pathways on the interior shelf (around Hanna Shoal). In that scenario, our survey
202 captured the “front” between the RWW, which previously had been streaming out of the
203 canyon from the coastal pathway, and the PWW that arrived later via the longer pathway.
204 Below we shed light on this issue by investigating the mixing implied by the measurements,
205 and the timing of the PWW pathways using the numerical model.

206 4. Measurements in Barrow Canyon

207 Based on the observed wind forcing and TS measurements, we consider the CTD transects
208 $BC_1(a)$, BC_2 , BC_3 , and BC_4 to be quasi-synoptic. Before presenting the analysis of these
209 sections, we first compare transects $BC_1(a)$ and (b) , which demonstrate how advection from
210 upstream sources can profoundly influence the region on short timescales.

211 4.1. Comparison of Upper Canyon Transects

212 Figure 5 compares the vertical sections of temperature and alongstream velocity for the
213 two BC_1 transects, which were separated by roughly one week. In both cases, the near-
214 surface water is relatively warm ($> 3^\circ\text{C}$) and the maximum current speed is in excess of
215 0.5 m s^{-1} . However, pronounced differences are apparent in the two sections. The 29 July
216 2009 transect consisted largely of PWW. (In this figure and others to follow, the PWW
217 corresponds to the dark blue and purple colors, i.e. colder than -1.65°C .) By contrast, the
218 6 August 2009 transect recorded the presence of very warm Alaskan Coastal Water at the
219 western four stations, extending as deep as 80 m. The structure of the down-canyon flow
220 was also markedly different between the two realizations. The 29 July current was more

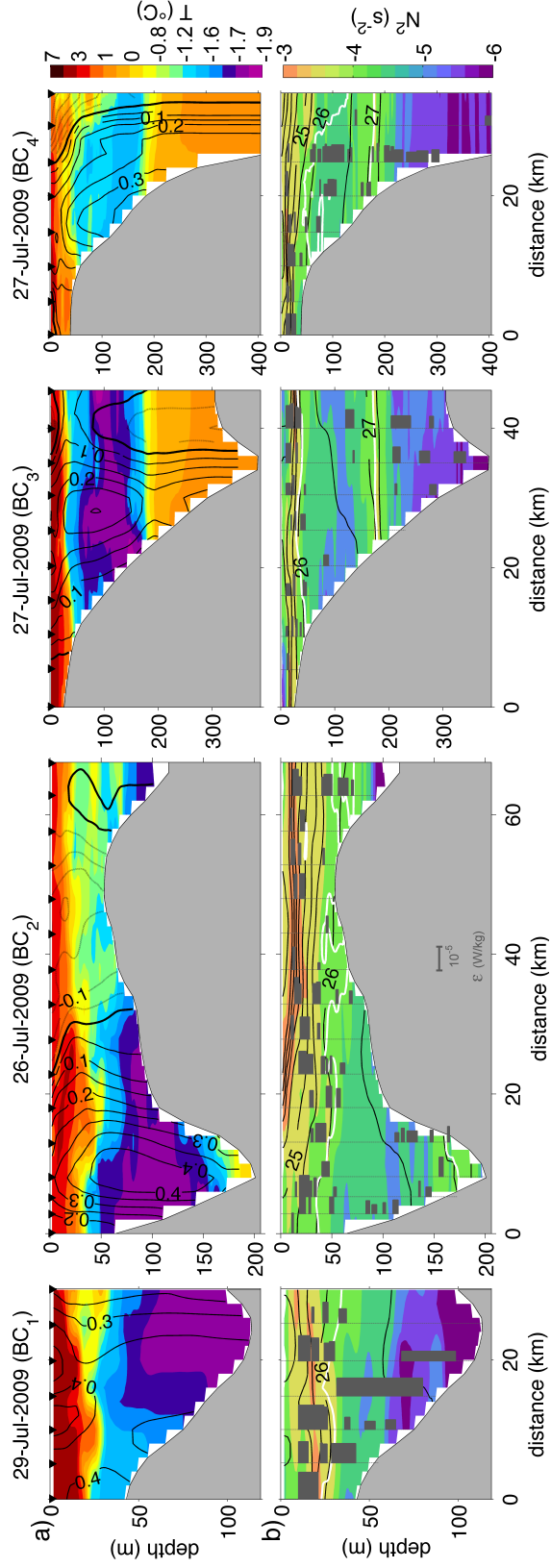


Figure 7: a) Temperature (color) overlain by velocity (contours, m/s) and b) stratification (color) for the BC₁(a), BC₂, BC₃, BC₄ transects. In panel b, the thick white contours denote the -1.2°C isotherms which approximately bracket the Pacific winter water layer; the black contours are density kg m^{-3} . The turbulent kinetic energy dissipation rate (from a Thorpe scale analysis) is indicated by the grey bars.

221 barotropic, and the 6 August current was strongly baroclinic. It is clear that the ACC was
222 present on the western flank of the canyon during the second realization.

223 During the re-occupation of this section, measurements were taken beyond the canyon
224 rim onto the Chukchi shelf (Fig. 2). Offshore, the section shows a surface-intensified,
225 southward-flowing current associated with a hydrographic front just beyond the western
226 wall of the canyon. The swift part of the current is advecting warm water, while the base
227 of the jet contains PWW. We suspect that this is the Pacific Water pathway that extends
228 northward through Central Channel and bends anti-cyclonically around Hanna Shoal (see
229 Fig. 1). Note that the southward-flowing PWW is not constrained to the shelf region between
230 Hanna Shoal and Barrow Canyon, i.e. a portion extends down into the canyon (Fig. 5 b).
231 This signature may be the eastward-flowing Chukchi shelfbreak jet being diverted along the
232 isobaths into Barrow Canyon. This interpretation is also consistent with the southward flow
233 along the western half of BC_2 (Fig. 2). In any event, these flows provide a source of PWW
234 into Barrow Canyon late in the season, well after the Alaskan coastal pathway would have
235 advected such cold water through the canyon (see also Pickart et al., this issue).

236 The change from the down-canyon flow of PWW in the first realization to the appearance
237 of the ACC in the second realization is clearly associated with advection from the Chukchi
238 shelf. Mooring data from within Barrow Canyon suggest that this transition can be quite
239 abrupt. For example, (Mountain et al., 1976) note an increase of 4.5°C in less than 48 hours.
240 The comparison above highlights one of the difficulties in treating shipboard sections acquired
241 in this region as synoptic, especially when the timing of those sections is not consistent with
242 the progression of the flow. Temporally, we sampled in the following order: BC_2 , BC_4 ,
243 BC_3 , and $BC_1(a)$ due to logistical constraints imposed by mooring operations on the cruise.
244 While this is not ideal, analysis of the transports and properties (Section 4.2) supports the
245 assumption of near-synopticity for these four transects.

246 *4.2. Evolution of the Flow through Barrow Canyon*

247 We begin the analysis of how the flow evolves through the canyon by considering volume
248 transports separated into TS classes for the four near-synoptic sections (Fig. 6a). For this

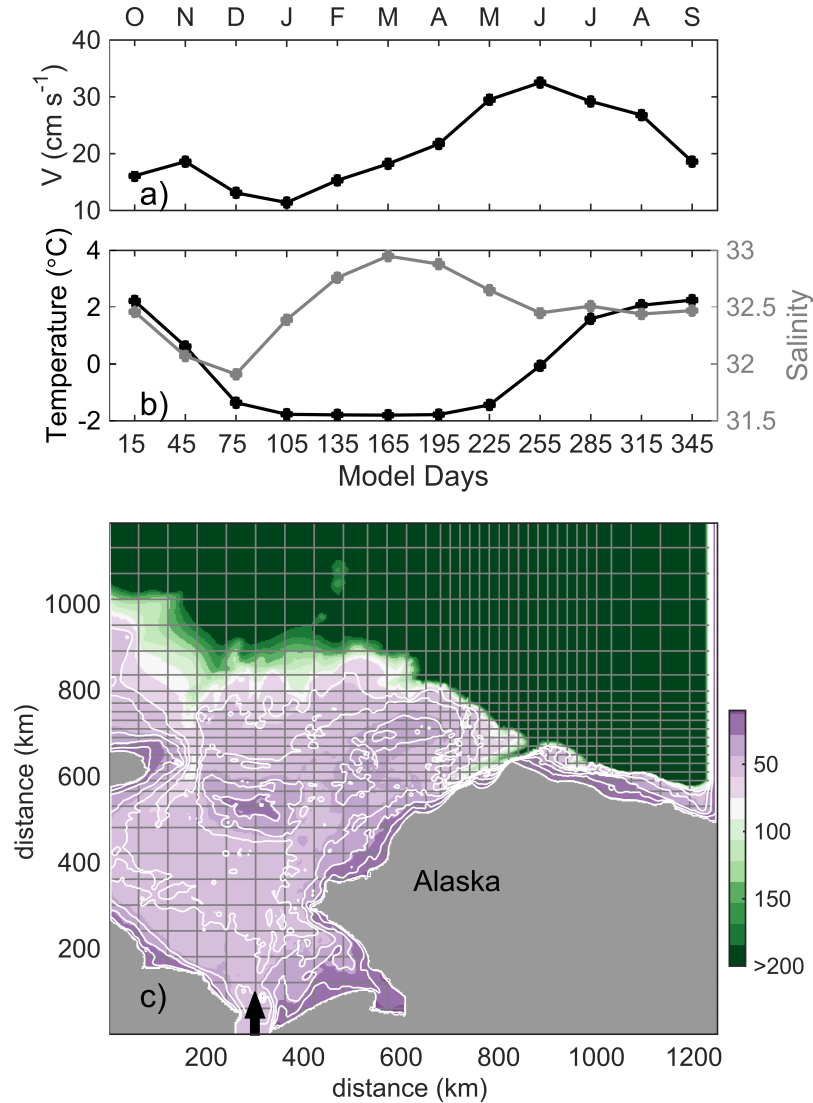


Figure 8: Model forcing and domain. The seasonal cycle model is forced at Bering Strait with a spatially-homogeneous signal in a) velocity and b) temperature-salinity. The model domain (c) is non-uniform, with the highest lateral resolution centered in Barrow Canyon. Grid boundaries are plotted in grey at an interval of 20 cells. The bathymetry (m) is colored, with contours plotted every 10 m from 10 to 60 m depth in white.

249 analysis, positive transports are directed out of the Chukchi Sea, and water mass classes were
 250 defined based on the character of the TS plots. A representative TS diagram from BC_2 is
 251 shown in Fig. 6c. As discussed above, water with temperature less than -1°C was classified

252 as winter water (PWW or RWW). Water warmer than this limit was sorted into three groups:
253 modified meltwater (MW), summer water (SW, predominantly Bering summer water), and
254 Atlantic water (AW). The first two classes are separated from AW using a constant salinity of
255 33. A linear relation between temperature and salinity (diagonal line shown in Fig. 6c) was
256 used to separate SW and MW, with the fresher, colder branch being attributed to MW. We
257 note that various TS definitions have been applied in the literature to describe the regional
258 water masses of the Chukchi and Beaufort Seas in detail. The boundaries adopted here
259 are meant to characterize the broad water types; small variations to these definitions do
260 not change our conclusions given the types of water sampled in this shipboard survey. The
261 combination of the two winter water masses is referred to below as WW.

262 The total transport of WW and SW out of the Chukchi Sea (i.e., the sum of the positive
263 bars for each transect) was nearly identical for $BC_1(a)$ and BC_2 at 0.85 Sv, and slightly less
264 for BC_3 and BC_4 at ~ 0.65 Sv and 0.58 Sv, respectively. We note that BC_3 and BC_4 also
265 transported roughly 0.08 Sv and 0.17 Sv of AW in the upper 250 m; these values are not
266 represented in Fig. 6a. (The transport of AW in $BC_1(a)$ and BC_2 is negligible.) BC_2 , which
267 was the only transect of this set that extended onto the Chukchi shelf offshore of Barrow
268 Canyon, shows transport of MW to the southwest. Although differences are apparent, the
269 relative amounts of SW (~ 0.2 Sv) and WW (~ 0.5 Sv) are consistent among these four
270 transects. The primary difference is that the winter water transport in the first three sections
271 consisted primarily of PWW, while in the fourth section it was comprised entirely of RWW
272 (Fig. 6b).

273 The evolution of the flow through the canyon is effectively visualized by comparing ver-
274 tical sections of the four transects (Fig. 7 with the -1.2°C isotherms in white delimiting the
275 WW). It is seen that SW is found near the surface in all of the sections. The first transect
276 $BC_1(a)$, in the upper portion of Barrow Canyon, is dominated by outflow of PWW that is
277 in contact with the bottom. The isopycnals are relatively flat and, as such, there is little
278 vertical structure to the flow. A marked transition takes place between this transect and
279 the next one (BC_2). One sees that the layer of PWW has descended and stretched so that

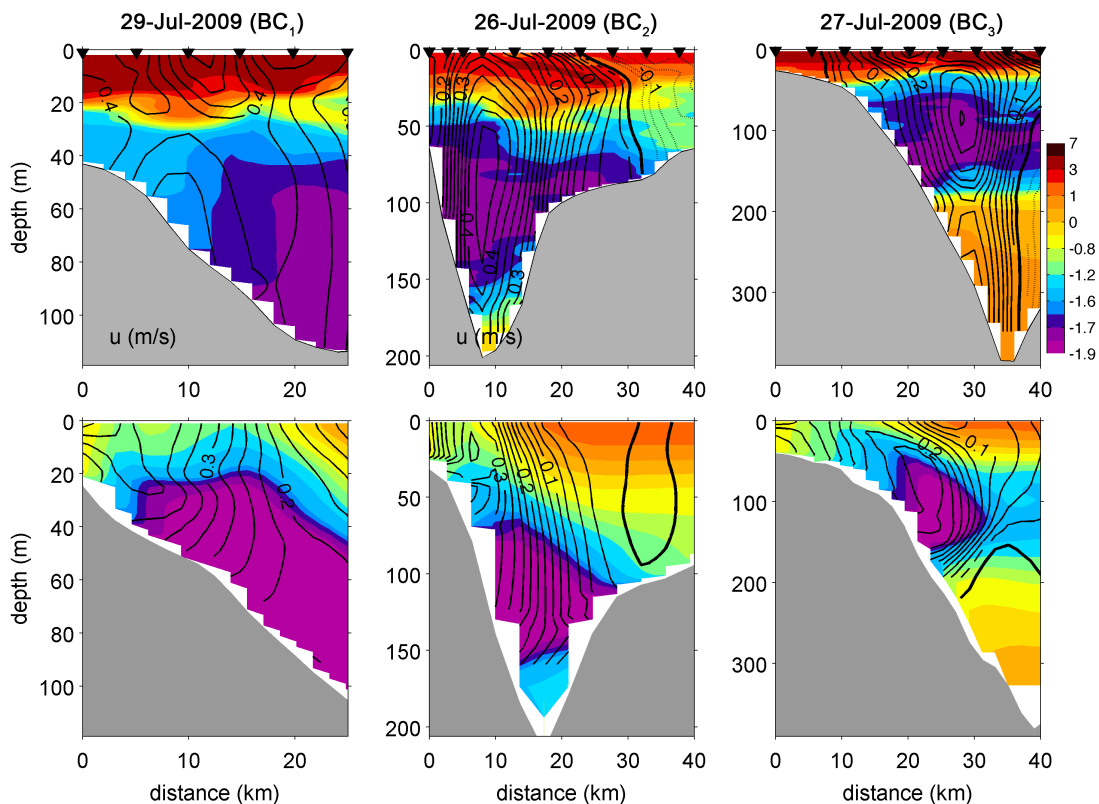


Figure 9: Comparison of the observations and the model along three transects through Barrow Canyon. The color is temperature ($^{\circ}\text{C}$) and the contours are alongstream velocity (m/s). The model transects were sampled along similar latitude and longitude lines.

280 it now extends down to 150 m, lying above the deep Atlantic layer. The other significant
 281 change is that the isopycnals that bound the PWW are now strongly sloped. In particular,
 282 they diverge as one progresses from the western side of the canyon to the eastern side. This
 283 results in a mid-depth intensified jet. Interestingly, at the offshore end of this transect there
 284 is weak flow of PWW approaching Barrow Canyon along the Chukchi slope. This supports
 285 the notion that some of the PWW seen progressing into the canyon in section $BC_1(b)$ has
 286 emanated from the Chukchi shelfbreak jet.

287 The third transect, BC_3 , is at the canyon mouth (Fig. 2), and the conditions here are not
 288 very different from the preceding section. The PWW layer is similar in structure and the cold

	BC ₁ (a)	BC ₂	BC ₃	BC ₄
Min	$8.4 \cdot 10^{-9}$	$4.4 \cdot 10^{-9}$	$2.0 \cdot 10^{-8}$	$1.2 \cdot 10^{-8}$
Max	$6.6 \cdot 10^{-5}$	$5.3 \cdot 10^{-5}$	$2.1 \cdot 10^{-5}$	$2.8 \cdot 10^{-5}$
Median	$9.8 \cdot 10^{-7}$	$1.4 \cdot 10^{-6}$	$6.5 \cdot 10^{-8}$	$6.5 \cdot 10^{-7}$
Mean	$8.7 \cdot 10^{-6}$	$5.7 \cdot 10^{-6}$	$1.4 \cdot 10^{-6}$	$3.0 \cdot 10^{-6}$

Table 1: Turbulent kinetic energy dissipation estimates for BC₁(a), BC₂, BC₃, BC₄ transects in W kg^{-1} from the Thorpe Scale analysis. The means and medians are calculated for detectable values over the water column; they will be high given that low values of ϵ are not included in the estimate.

289 jet remains mid-depth intensified. More of the Atlantic layer is sampled in this section, and
290 there is a reversal in the deep isopycnal slope associated with an enhanced flow of this warm
291 water in the same direction as the PWW. The final transect BC_4 is beyond the canyon and
292 crosses the Beaufort slope. Again there is marked change, both in the hydrography and in
293 the flow. Notably, there is no PWW present in the section, only RWW. Also, the isopycnals
294 are now uniformly sloped so that the sense of thermal wind shear is the same throughout
295 the water column; accordingly, the jet of cold water is now bottom trapped. Note that the
296 strongest flow of winter water is found roughly 100 m deeper at BC_4 than at the previous
297 two sections (~ 180 m versus ~ 80 m). Overall then, our survey showed that the flow of
298 winter water emanating from Barrow Canyon moderated in its properties – changing from
299 PWW to RWW – and transitioned from a nearly barotropic structure at the canyon head
300 to being mid-depth intensified, and, finally, becoming bottom-intensified along the Chukchi
301 slope.

302 The turbulent kinetic energy dissipation from the four transects is estimated using a
303 Thorpe scale analysis (Figure 7b) with the intent of bounding the degree of mixing between
304 SW and PWW within Barrow Canyon. The use of Thorpe scales limits the calculation
305 of dissipation to regions where resolved overturns are detected and, consequently, sets a
306 minimum on the observable dissipation rate. Even though energy constraints suggest that
307 overturns occur more easily in weak stratification, they are more difficult to detect given

308 the resolution of the CTD. Accordingly, a tendency for enhanced dissipation to occur in
309 regions of increased stratification is evident in Fig. 7b. Mean, median, and extreme values
310 are presented in Table 1. Note that the means and medians would be considerably lower
311 if we replaced non-resolvable values with a “noise floor”, e.g., 10^{-10} W kg $^{-1}$. Regardless of
312 any relative sensitivity, in this series of transects the mixing between summer and winter
313 water tended to be greatest in the upper to mid canyon and decreased as the water transited
314 through the mouth.

315 Dissipation can be converted to a turbulent diffusivity using $K = \Gamma\epsilon/N^2$ with the mixing
316 efficiency Γ assumed to be equal to 0.2. This relationship yields an upper bound on the
317 mean K within ± 5 m of the upper -1°C isotherm (i.e., the SW/WW boundary) of roughly
318 5×10^{-4} m 2 s $^{-1}$ over the upper three transects. Diffusivity along BC $_4$ is considerably lower
319 at 10^{-7} m 2 s $^{-1}$. (For the mean estimates of diffusivity a molecular noise floor is assumed.)
320 Assuming a constant diffusivity of 5×10^{-4} m 2 s $^{-1}$ applied to an interface between SW at
321 nominally 4°C and PWW at nominally -2°C , a one-dimensional mixing model suggests
322 that a roughly 10-m layer of RWW can be created over one day (roughly equivalent to the
323 advective timescale for the transit between BC $_1$ (a) and BC $_2$). Note that this estimate is
324 merely illustrative of the potential for diapycnal mixing to be a significant contributor to
325 water mass evolution within the canyon. It is oversimplified, notably by neglecting pre-
326 existing gradients between SW and PWW (i.e., the initial condition is not two-layer), and in
327 the inability of sparse Thorpe-scale estimates to adequately resolve intermittent turbulent
328 events in order to yield robust mean mixing values. Nonetheless, despite these limitations,
329 this simple estimate strongly suggests that the abrupt transition between PWW and RWW
330 observed between BC $_3$ (a) and BC $_4$ in the shipboard survey did not result from vertical
331 mixing.

332 5. Comparison to the Idealized Model

333 The MIT general circulation model (MITgcm; Marshall et al., 1997) was used to formu-
334 late a regional oceanic model of the Chukchi Sea with realistic bathymetry (International

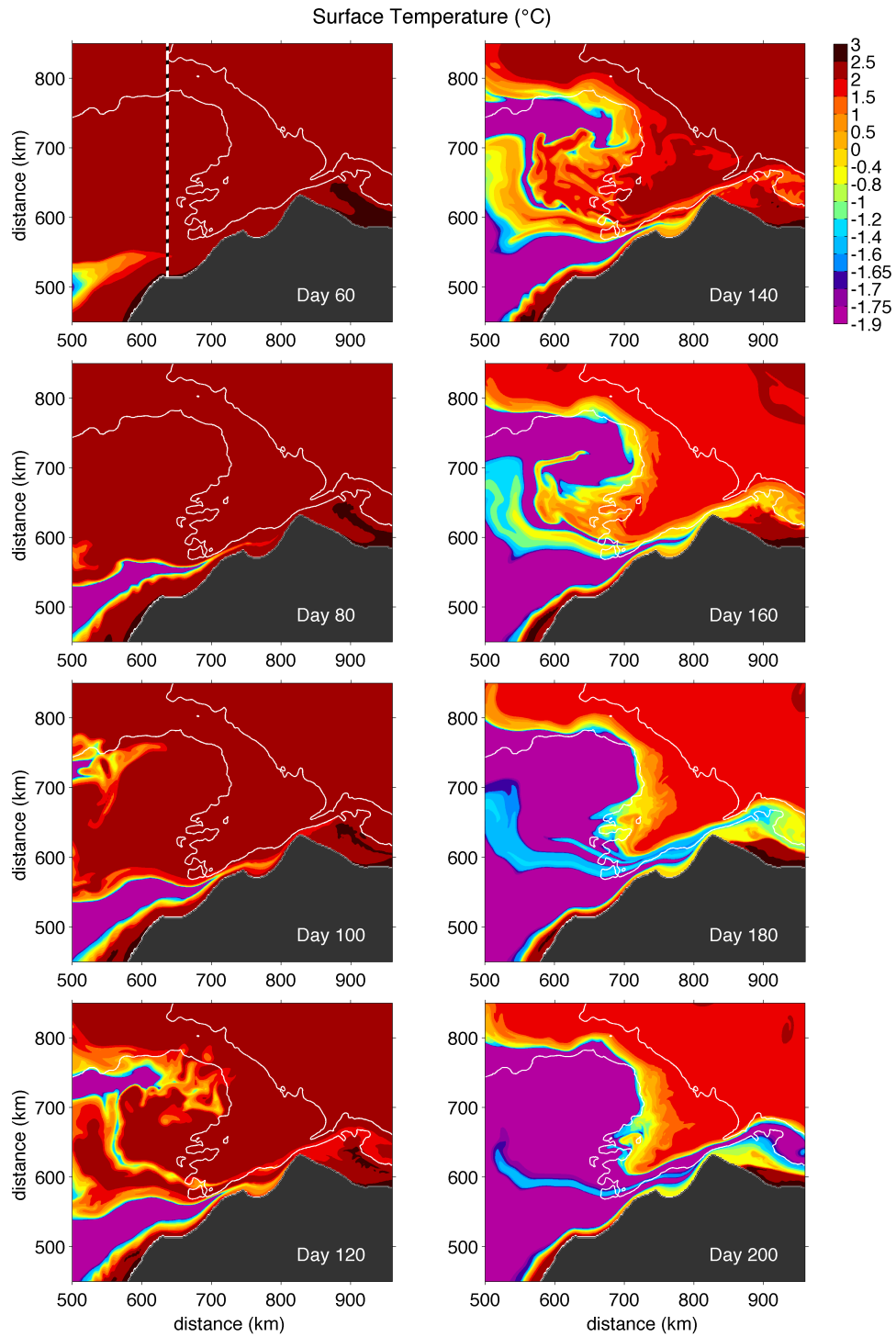


Figure 10: Surface temperature (color, °C) at specified model days in the vicinity of Barrow Canyon for the winter water simulation. The 50 and 200-m isobaths are plotted in white.

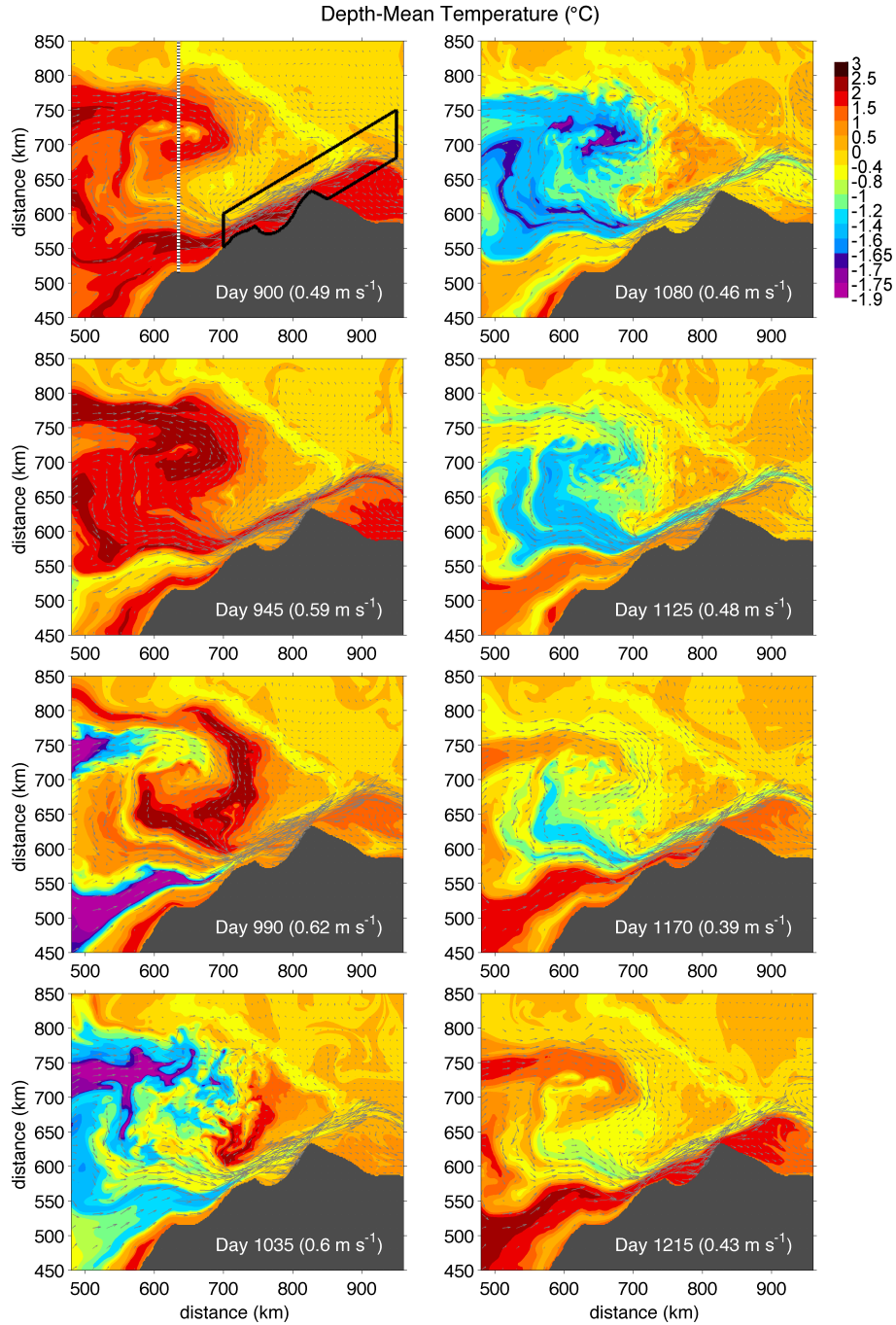


Figure 11: Depth-mean temperature (color, $^{\circ}\text{C}$) in the vicinity of Barrow Canyon during the third year of the seasonal cycle simulation. The vectors denote the depth-mean velocity with maximum speeds indicated in the lower right corner. The upper left panel shows the transect line used in Fig. 12 (white dashed) and the averaging area used for Fig. 13 (black box).

335 Bathymetric Chart of the Arctic Ocean 3.0, Jakobsson et al., 2012). The horizontal resolution
336 varied from 1-3 km, with the highest resolution centered in Barrow Canyon (Fig. 8). A 2-m
337 vertical resolution was used within the upper 125 m of the water column; deeper than this,
338 the resolution varied smoothly to a maximum cell size of 50 m at the model bottom depth of
339 525 m (Fig. 8c). The model employed a grid-dependent horizontal viscosity; typical values
340 were around $10 \text{ m}^2\text{s}^{-1}$. The horizontal diffusivity was set to zero. A Mellor-Yamada (Mellor
341 and Yamada, 1982) vertical mixing scheme was used with a background viscosity/diffusivity
342 of $10^{-5} \text{ m}^2\text{s}^{-1}$. The model was initialized from rest with a horizontally uniform temperature
343 and salinity profile created from a combination of historical CTD data for water on the shelf
344 and ice-tethered profiler data for deeper water (Toole et al., 2011).

345 The eastern and western model boundaries are closed. The model was forced with a
346 prescribed flow at the southern (Bering Strait) and northern boundaries. At both open
347 boundaries the model temperature, salinity, and velocity are restored to prescribed values
348 over 15 grid cells using a time constant that varied linearly from 10 days (innermost grid
349 cell) to 1 day (outer grid cell) over the restoring region. At the northern boundary the
350 temperature and salinity were restored to the initial conditions, and the northward velocity
351 was set to a weak depth-uniform outflow that balanced the inflow at Bering Strait. The
352 model is primarily forced through the southern boundary. Two simulations are considered
353 here. The first, referred to as the winter water run, uses constant forcing at the Bering Strait
354 defined by a uniform northward velocity of 0.2 m s^{-1} importing water near the freezing point
355 at a salinity of 32.5. (Simulations with smaller and larger transports were also carried out, the
356 effect of which was to lengthen/shorten the time required for the transport of winter water
357 through the Chukchi Sea.) The winter water simulation was run for 540 days. The second
358 simulation considers a seasonal cycle in velocity, temperature, and salinity (Fig. 8a and b)
359 according to Woodgate et al. (2005). (We assume no spatial variation across Bering Strait.)
360 The climatological seasonal simulation is started in October to match the initial salinity and
361 temperature profiles throughout the domain and was run for a total of 1260 days. Model
362 days 15, 375, 735, and 1095, therefore, correspond to mid-October each simulation year (Fig.

363 8a and b).

364 Both simulations are formulated to consider questions related to the timing of trans-
365 port pathways across the Chukchi shelf in the absence of external forcing, i.e., neglecting
366 winds, tides, and surface heat/salt fluxes. As such, the seasonality in the model will differ
367 from that in the observations. Importantly, however, the advective component of the model
368 seasonal cycle driven by the Bering Strait inflow is unambiguous within the present model
369 configuration. This allows us to robustly diagnose the travel times along the various path-
370 ways. Despite its simplifications, the model captures essential aspects of the observations
371 in the vicinity of Barrow Canyon. In particular, the simulated current transitions from a
372 primarily barotropic flow near the head of the canyon to a baroclinic flow with a subsurface
373 maximum near the mouth of the canyon, as is the case for the observations (Fig. 9). In the
374 model, this transition occurs as the dense winter water sinks to its level of neutral density
375 as it travels down canyon. In other words, the density range encompassing the winter water
376 mode (density between 26.5 and 26.8 kg m^{-3}) resides at an average depth of roughly 90 m
377 in the open Beaufort Sea. (Recall that the model is initialized based on the observations,
378 so that the observed down-canyon density field is similar to the modeled.) The winter wa-
379 ter simulation is also consistent with our assumption that the observed transects $BC_1(a)$,
380 BC_2 , and BC_3 are quasi-synoptic, given the similarity between the observed and modeled
381 currents and temperature. We now use the winter water simulation to identify pathways of
382 topographically steered flow in the vicinity of Barrow Canyon. We then consider the timing
383 and co-existence of different water masses in Barrow Canyon using the seasonal simulation.

384 *5.1. Transport Pathways in the Vicinity of Barrow Canyon*

385 The winter water simulation (Fig. 10) highlights the multiple transport pathways dic-
386 tated by the topography in the Chukchi Sea: a rapid route along the Alaskan coast, a slower
387 route that circulates around the northern side of Hanna Shoal, and a third branch that diverts
388 eastward around the southern side of Hanna Shoal. These different pathways are readily seen
389 in the evolution of sea surface temperature (Fig. 10). The coastal branch and the clockwise
390 circulation around the north side of Hanna Shoal have been recognized previously in models

391 (e.g., Winsor and Chapman, 2004; Spall, 2007) and observations (Weingartner et al., 2013).
392 Only recently has a pathway of WW around the southern side of Hanna Shoal been revealed
393 by late-spring/early-summer shipboard measurements (Pickart et al., 2016; Pacini et al., this
394 issue). Our model confirms such a cyclonic circulation south of the shoal (Fig. 10).

395 Consistent with the model of Winsor and Chapman (2004), the transit time along the
396 coastal pathway is roughly 6 months. The WW in the central shelf pathway that is diverted
397 south of Hanna Shoal reaches Barrow Canyon several months later, and roughly a month
398 after this the WW in the northernmost route arrives in the canyon. Although these exact
399 arrival times depend on the strength of the forced flow through Bering Strait, the arrival
400 sequence is insensitive to the magnitude of the inflow (i.e., the coastal pathway is the fastest
401 and the northern route around Hanna Shoal is the slowest.)

402 The eastward transport across a north-south line extending from the Alaskan coast over
403 the top of Hanna Shoal upstream of the mouth of Barrow Canyon ($x = 635$ km, see the
404 first panel of Fig. 10), indicates that the northern route around Hanna Shoal transports
405 slightly less than half of the water (40%) that eventually drains into Barrow Canyon, with
406 the southern two branches carrying the remaining 60%. Of this remainder, the majority of
407 the water ($\sim 75\%$) is transported along the coastal pathway. While the total transport is
408 sensitive to inflow conditions at Bering Strait, the relative ratio is consistent for the uniform
409 winter water simulations. For a constant inflow of 0.20 m s^{-1} , the total eastward transports
410 are 0.6 Sv for the combined coastal and southern Hanna Shoal routes and 0.4 Sv for the
411 northern Hanna Shoal pathway. Based on data from an early-summer shipboard survey of
412 the northeast Chukchi Sea, Pickart et al. (2016) deduced ~ 0.8 Sv for the combined coastal
413 and southern Hanna Shoal branches, and ~ 0.2 Sv for the northern pathway.

414 *5.2. Advective Seasonality of Water Masses within Barrow Canyon*

415 The seasonal simulation allows for interpretation of the advective contribution to the
416 seasonal cycle in the vicinity of Barrow Canyon in the absence of surface forcing (Fig. 11).
417 The yearly progression of water mass arrival at a particular location is repeated in each model
418 year with only slight variability in timing (order one week). Notably, the same characteristic

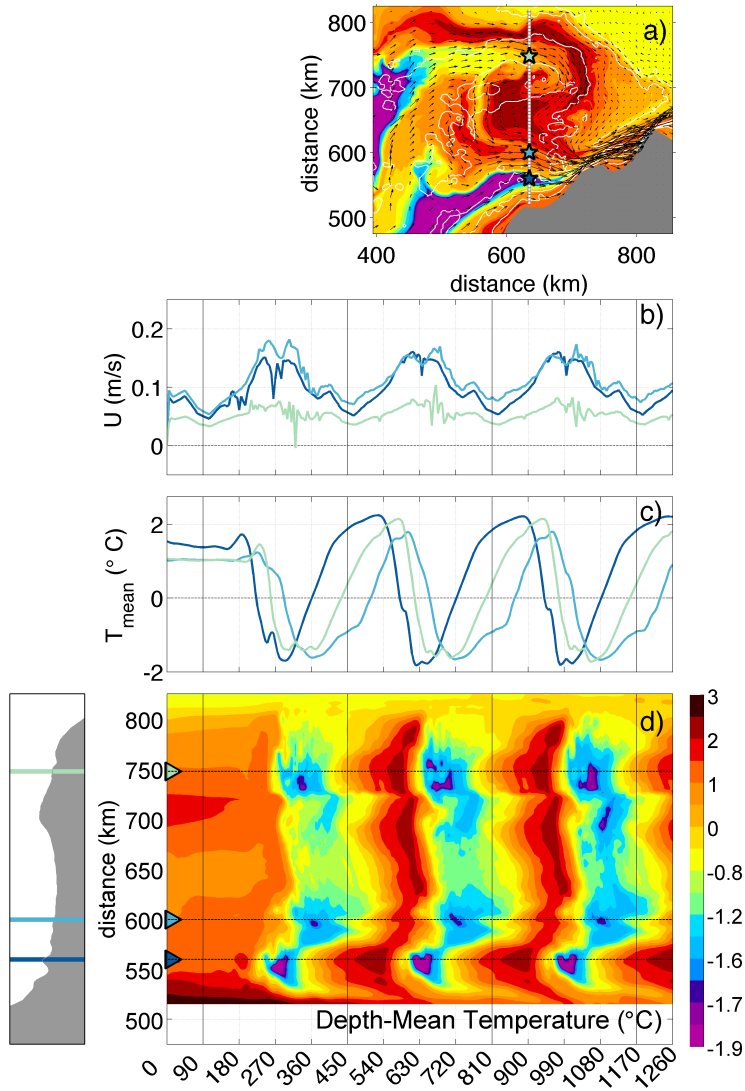


Figure 12: a) Overhead map showing the depth mean temperature (color, °C) in mid-June (model day 615). b) Time series of depth-mean eastward velocity and c) temperature at a sequence of locations progressing offshore of Alaska along a north-south transect upstream of Barrow Canyon and crossing over Hanna Shoal ($x = 635$ km, white dashed line in panel a). The time series locations are indicated by stars on the overhead map and horizontal lines on the bathymetric section (lower left); these locations were selected within the coastal pathway (dark blue), the southern Hanna Shoal pathway (cyan), and the northern Hanna Shoal pathway (light green). d) Depth-mean temperature (color, °C) as a function of time and transect distance.

419 pathways along the Alaskan coast and around the two sides of Hanna Shoal are delineated
 420 by arrival of both winter water (e.g., day 1035 in Fig. 11) and summer water (e.g. day 1215

421 in Fig. 11).

422 The advective time scales for the various pathways can be estimated by the time lag
423 between the temperature at Bering Strait and the temperature downstream at specific loca-
424 tions in the Chukchi Sea. We consider three locations along the meridional line at $x=635$ km
425 corresponding to the three pathways discussed above (Fig. 12a). The temperature along
426 the northern Hanna Shoal pathway, the southern Hanna Shoal pathway, and the coastal
427 pathway lags the forcing at Bering Strait by 200, 240, 150 days, respectively (Fig. 12c and
428 d). The water carried along the northern Hanna Shoal route requires an additional \sim month
429 to circulate clockwise around the eastern side of the shoal. From here, the northern branch
430 must still retroreflect and turn back to the east before reaching Barrow Canyon. Thus, the
431 overall transit time through the Chukchi Sea when there is no heat exchange at the air-sea-
432 ice interface leads to a seasonal cycle that is \gtrsim 6 months out of phase with Bering Strait.
433 In contrast to temperature (i.e., water type), the volume transports along each of the three
434 pathways are roughly in phase with one another and vary directly with the seasonal forcing
435 at Bering Strait (Fig. 12b). The transport adjusts nearly instantaneously across the shelf via
436 barotropic wave propagation. (The correlations and lags mentioned above are all significant
437 with $R \geq 0.75$.)

438 The time lag between the multiple pathways results in summer and winter waters regu-
439 larly co-existing in the vicinity of Barrow Canyon; in fact, this is the case over the majority of
440 the year in the model (Figs. 11 and 12). For example, as the coastal pathway transitions to
441 summer water in the canyon, relatively cool waters are located mid-shelf (Fig. 11 day 1080).
442 This is consistent with the observations of Pickart et al. (2016) who observed summer water
443 in Barrow Canyon at the same time that winter water was rounding both sides of Hanna
444 Shoal.

445 Although the lack of surface forcing limits realism of the overall model seasonal cycle,
446 the simulation does indicate that winter water first arrives in the canyon via the coastal
447 pathway, followed some time later by a second occurrence via the interior pathways. This is
448 in line with the measurements of Weingartner et al. (in press) and Pickart et al. (this issue).

449 The modeled transition is demonstrated by a succession of snapshots from the simulation
450 showing the PWW front progressing down the canyon due to the later arriving PWW from
451 the Hanna Shoal pathways (Fig. 13). Such a rapid transition between water types draining
452 through Barrow Canyon also offers an explanation of the abrupt change from RWW to
453 PWW in the boundary current observations presented here (Fig. 7). Thus, we can state
454 with confidence that the alongstream warming of the winter water observed in our shipboard
455 survey is advective in nature and not the result of mixing as the current progresses into the
456 Beaufort Sea.

457 6. Conclusions

458 Observations, supported with output from an idealized model of the Chukchi Sea, high-
459 light the dependence of hydrographic conditions within and downstream of Barrow Canyon
460 on the advective pathways across the Chukchi shelf. Specifically, the analyses presented
461 here suggest that the seasonality of water masses within Barrow Canyon is closely tied to
462 the seasonality of the Bering Strait inflow lagged by the relative transit times along three
463 primary pathways that feed the canyon: a coastal pathway, a southern Hanna Shoal path-
464 way, and a northern Hanna Shoal pathway. Due to the variable transit times, summer and
465 winter water masses regularly occupy Barrow Canyon at the same time. The re-occupation
466 of the upstream canyon transect ($BC_1(a)$) is especially illustrative of how different pathways
467 advecting different water types converge within the canyon. In this case, warm Alaskan
468 coastal water occupied the coastal pathway, while cold newly ventilated Pacific Winter Wa-
469 ter (PWW) occupied the offshore flank of the canyon, having emanated from one or both of
470 the Hanna Shoal pathways.

471 Analyses of wind, temperature-salinity properties, and transports suggest that the se-
472 quence of shipboard transects capturing the downstream evolution of winter water within
473 Barrow Canyon could be treated as near-synoptic. As winter water travels down canyon
474 the current adjusts from a nearly barotropic structure to one with pronounced baroclinicity
475 characterized by a sub-surface maximum in velocity. The other notable change progressing

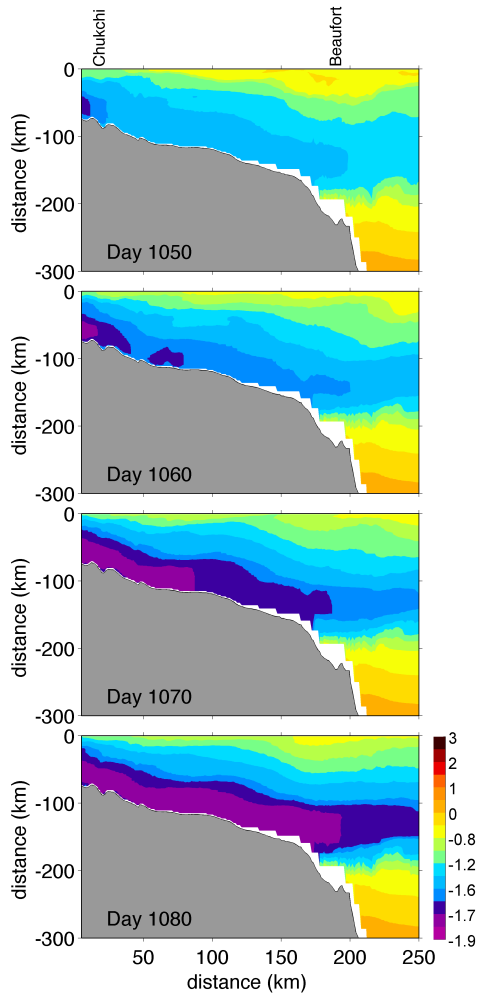


Figure 13: Along-canyon progression of the across-canyon minimum temperature, showing the transition from RWW advected by the coastal pathway (top) to PWW carried along interior pathways (bottom). An overhead view of the cross-sectional area is shown in the upper-left panel of Fig. 11.

476 downstream was in the type of winter water mode that occupied each transect; the three up-
 477 stream canyon transects ($BC_1 - 3$) primarily consisted of PWW, whereas BC_4 at the canyon
 478 mouth contained mostly remnant winter water (RWW). While one might envision that this
 479 transition could be ascribed to alongstream mixing of PWW, Thorpe scale estimates of
 480 turbulent diffusivity suggest that such a scenario is unlikely.

481 Instead, we argue that the abrupt transition to RWW along the Pacific water pathway
 482 relates to the timing of the transects and drainage of different water types from the multiple

483 pathways feeding Barrow Canyon. The mouth transect (BC_4) was sampled roughly a day
484 after BC_2 , a day prior to BC_3 , and several days prior to $BC_1(a)$. Given the advective
485 time scales through the canyon, BC_4 was effectively sampled first in a synoptic frame. An
486 alternative interpretation, supported by the seasonal simulation, is that PWW travelling
487 along one (or both) of the interior shelf pathways (BC_{1-3}) was trailing RWW carried along
488 the coastal pathway (BC_4). The model suggests that such a transition occurs on the order
489 of one week, while the observations indicate that it can happen in a matter of days.

490 Even though the above analyses suggest that local diapycnal mixing does not solely
491 create the observed RWW, the Thorpe scale estimates of dissipation and diffusivity are not
492 negligible – just insufficient to locally produce the observed volume of RWW. Mixing (both
493 isopycnal and diapycnal) may have other important, yet more subtle, consequences. For
494 example, given that a portion of the water emanating from Barrow Canyon moves directly
495 into the deep Canada Basin and Beaufort Sea, local turbulent buoyancy fluxes may modify
496 how and where the Arctic halocline is ventilated. Furthermore, since topographically steered
497 waters have different origins as well as advective histories, dissimilar water types that co-exist
498 in the canyon will likely be distinguished by properties other than temperature and salinity,
499 such as carbon and nutrients. Turbulent flux divergence may therefore be an important
500 contributor to other tracer budgets. For example, a straightforward extension is that mixing
501 between nutrient replete and deplete waters may help sustain this biologically productive
502 region (e.g., Grebmeier et al., 2006). The combination of advection leading to heterogenous
503 water properties over a constrained geographic region, and local mixing acting on pronounced
504 gradients, lead to the potential for Barrow Canyon to play a central role in regional water
505 mass modification.

506 **Acknowledgements**

507 The authors thank Terry McKee for calibrating the hydrographic data and Frank Bahr
508 for processing the shipboard ADCP data set. ES was supported as a WHOI Postdoctoral
509 Scholar through the WHOI Ocean and Climate Change Institute. RP was funded by the

510 National Science Foundation under grant PLR-1303617.

511 **References**

512 Aagaard K, Roach AT. Arctic ocean-shelf exchange: Measurements in Barrow Canyon. *J*
513 *Geophys Res* 1990;95:18163–75. doi:10.1029/JC095iC10p18163.

514 Bourke RH, Paquette RG. Atlantic Water on the Chukchi Shelf. *Geophys Res Lett*
515 1976;3(10):629–32.

516 Brugler ET, Pickart RS, Moore GWK, Roberts S, Weingartner TJ, Statscewich H. Sea-
517 sonal to interannual variability of the Pacific water boundary current in the Beaufort Sea.
518 *Progress in Oceanography* 2014;127:1–20.

519 Coachman LK, Aagaard K, Tripp RB. Bering Strait: The regional physical oceanography.
520 University of Washington Press, 1975.

521 Corlett W, Pickart RS. The Chukchi Slope Current. *Progress in Oceanography* 2017;153:50–
522 6.

523 Dillon TM. Vertical overturns: A comparison of Thorpe and Ozmidov length scales. *J*
524 *Geophys Res* 1982;87(C12):9601–13.

525 Galbraith PS, Kelley DE. Identifying overturns in CTD profiles. *J Atmos Ocean Technol*
526 1996;13:688–702.

527 Gong D, Pickart RS. Summertime circulation in the eastern Chukchi Sea. *Deep Sea Research*
528 *Part II: Topical Studies in Oceanography* 2015;118:18–31.

529 Grebmeier JM, Cooper LW, Feder HM, Sirenko BI. Ecosystem dynamics of the Pacific-
530 influenced Northern Bering and Chukchi Seas in the Amerasian Arctic. *Progress in*
531 *Oceanography* 2006;71:331–61. doi:10.1016/j.pocean.2006.10.001.

532 Itoh M, Shimada K, Kamoshida T, McLaughlin F, Carmack E, Nishino S. Interannual
533 variability of Pacific Winter Water inflow through Barrow Canyon from 2000 to 2006. *J*
534 *Oceanogr* 2012;68:575–92. doi:10.1007/s10872-012-0120-1.

535 Jakobsson M, Mayer L, Coakley B, Dowdeswell JA, Forbes S, Fridman B, Hodnesdal H,
536 Noormets R, Pedersen R, Rebesco M, Schenke HW, Zarayskaya Y, Accettella D, Arm-
537 strong A, Anderson RM, Bienhoff P, Camerlenghi A, Church I, Edwards M, Gard-
538 ner JV, Hall JK, Hell B, Hestvik O, Kristoffersen Y, Marcussen C, Mohammad R,
539 Mosher D, Nghiem SV, Pedrosa MT, Travaglini PG, Weatherall P. The International
540 Bathymetric Chart of the Arctic Ocean (IBCAO) Version 3.0. *Geophysical Research*
541 *Letters* 2012;39(12). URL: [http://dx.doi.org/10.1029/](http://dx.doi.org/10.1029/2012GL052219)
542 [2012GL052219](http://dx.doi.org/10.1029/2012GL052219).

543 Ladd C, Mordy CW, Salo SA, Stabeno PJ. Winter water properties and the Chukchi polynya.
544 *J Geophys Res* 2016;121:55165534.

545 Li M, Pickart RS. Circulation of the chukchi sea shelfbreak and slope from moored timeseries.
546 *Arctic Marine Science Symposium* 2017;Abstract, pg 85, [http://www.nprb.org/assets/](http://www.nprb.org/assets/amss/images/uploads/files/AMSS2017_BookofAbstracts.pdf)
547 [amss/images/uploads/files/AMSS2017_BookofAbstracts.pdf](http://www.nprb.org/assets/amss/images/uploads/files/AMSS2017_BookofAbstracts.pdf).

548 Lin P, Pickart R, Moore G, Spall M, Hu J. Characteristics and dynamics of wind-driven
549 upwelling in the Alaskan Beaufort Sea based on six years of mooring data. *Deep Sea Res*
550 *II* this issue;.

551 Marshall J, Adcroft A, Hill C, Perelman L, Heisey C. A finite-volume, incompressible Navier
552 Stokes model for studies of the ocean on parallel computers. *J Geophys Res* 1997;102:5753–
553 66. doi:10.1029/96JC02775.

554 Mellor GL, Yamada T. Development of a turbulence closure model for geophysical fluid
555 problems. *Rev Geophys Space Phys* 1982;20:851–75.

556 Mountain DG, Coachman LK, Aagaard K. On the flow through Barrow Canyon. *J Phys*
557 *Ocean* 1976;6:461–70. doi:{10.1175/1520-0485(1976)006<0461:OTFTBC>2.0.CO;2}.

558 Muench RD, Schumacher JD, Salo SA. Winter currents and hydrographic conditions on the
559 northern central Bering Sea shelf. *J Geophys Res* 1988;93:516–26.

560 Münchow A, Carmack EC. Synoptic Flow and Density Observations near an Arctic
561 Shelf Break. *J Phys Ocean* 1997;27:1402–19. doi:10.1175/1520-0485(1997)027<1402:
562 SFADON>2.0.CO;2.

563 Nikolopoulos A, Pickart RS, Fratantoni PS, Shimada K, Torres DJ, Jones EP. The western
564 arctic boundary current at 152 ° W: Structure, variability, and transport. *Deep Sea Res*
565 II 2009;56:1164–81.

566 Okkonen SR, Ashjian CJ, Campbell RG, Maslowski W, Clement-Kinney JL, Potter R. In-
567 trusion of warm Bering/Chukchi waters onto the shelf in the western Beaufort Sea. *J*
568 *Geophys Res* 2009;114(C13):0–+. doi:10.1029/2008JC004870.

569 Pacini A, Pickart R, Moore G, Nobre C, Bahr F, Vage K, Arrigo K. Characteristics and
570 transformation of pacific winter water on the Chukchi Sea shelf in late-spring. *Deep Sea*
571 *Res II* this issue;.

572 Padman L, Erofeeva S. A barotropic inverse tidal model for the Arctic Ocean. *Geophys Res*
573 *Let* 2004;31:2303. doi:10.1029/2003GL019003.

574 Pickart R, Moore G, Mao C, Bahr F, Nobre C, Weingartner T. Circulation of winter water
575 on the Chukchi shelf in early summer. *Deep Sea Res II* 2016;130:56–75.

576 Pickart R, Nobre C, Lin P, Arrigo K, Ashjian C, Berchok C, Cooper L, Grebmeier J, Hartwell
577 I, He J, Itoh M, Kikuchi T, Nishino S, Vagle S. Seasonal to mesoscale variability of water
578 masses and atmospheric conditions in Barrow Canyon, Chukchi Sea. *Deep Sea Res II* this
579 issue;.

580 Pickart RS, Stossmeister G. Outflow of Pacific water from the Chukchi sea to the Arctic
581 Ocean. *J Phys Ocean* 2008;10:135–48.

582 Pickart RS, Weingartner TJ, Pratt LJ, Zimmermann S, Torres DJ. Flow of winter-
583 transformed Pacific water into the Western Arctic. *Deep Sea Res* 2005a;52:3175–98.

584 Pickart RS, Weingartner TJ, Pratt LJ, Zimmermann S, Torres DJ. Flow of winter-
585 transformed Pacific water into the Western Arctic. *Deep Sea Res* 2005b;52:3175–98.
586 doi:10.1016/j.dsr2.2005.10.009.

587 Pisareva M, Pickart R, Fratantoni P, Weingartner T. On the nature of wind-forced upwelling
588 in Barrow Canyon. *Deep Sea Res II* this issue;.

589 Pisareva M, Pickart R, Spall M, Nobre C, Torres D, Moore G. Flow of Pacific water in
590 the western Chukchi Sea: Results from the 2009 RUSALCA expedition. *Deep Sea Res*
591 2015;105:53–73.

592 Schulze LM, Pickart RS. Seasonal variation of upwelling in the Alaskan Beaufort Sea: Impact
593 of sea ice cover. *Journal of Geophysical Research: Oceans* 2012;117(C6).

594 Shroyer EL. Turbulent kinetic energy dissipation in Barrow Canyon. *J Phys Oceanogr*
595 2012;42:1012–21. doi:10.1175/JPO-D-11-0184.1.

596 Shroyer EL, Plueddemann AJ. Wind-driven modification of the Alaskan coastal current. *J*
597 *Geophys Res* 2012;117(C03031). doi:10.1029/2011JC007650.

598 Spall MA. Circulation and water mass transformation in a model of the Chukchi Sea. *J*
599 *Geophys Res* 2007;112(C11):5025–+. doi:10.1029/2005JC003364.

600 Steele M, Morison J, Ermold W, Rigor I, Ortmeyer M, Shimada K. Circulation of summer
601 Pacific halocline water in the Arctic Ocean. *J Geophys Res* 2004;109(C02027). doi:10.
602 1029/2003JC002009.

603 Thorpe SA. Turbulence and mixing in a Scottish Loch. *Philos Trans Roy Soc London*
604 1977;286(1334):125–81.

- 605 Toole J, Krishfield R, Timmermans ML, Proshutinsky A. The Ice-Tethered Profiler: Argo
606 of the Arctic. *Oceanography* 2011;24(3):126–35.
- 607 Weingartner T. J. ea. Hydrographic variability over the northeastern Chukchi Sea shelf in
608 summer-fall 2008-2012. *Continental Shelf Research* 2012;;submitted.
- 609 Weingartner T, Aagaard K, Woodgate R, Danielson S, Sasakic Y, Cavalieri D. Circulation
610 on the north central Chukchi Sea shelf. *Deep Sea Res* 2005;52:3150–74.
- 611 Weingartner T, Dobbins E, Danielson S, Winsor P, Potter R, Statscewich H. Hydrographic
612 variability over the northeastern Chukchi Sea shelf in summer-fall 2008–2010. *Cont Shelf*
613 *Res* 2013;67:5–22.
- 614 Weingartner TJ, Cavalieri DJ, Aagaard K, Sasaki Y. Circulation, dense water formation,
615 and outflow on the northeast Chukchi shelf. *J Geophys Res* 1998;103:7647–62. doi:10.
616 1029/98JC00374.
- 617 Weingartner TJ, Potter R, Stoudt C, Dobbins E, Statscewich H, Winsor P, Mudge T, Borg
618 K. Transport and thermohaline variability in Barrow Canyon on the northeastern Chukchi
619 Sea shelf. *J Geophys Res* in press;.
- 620 Winsor P, Chapman DC. Pathways of Pacific water across the Chukchi Sea: A numerical
621 model study. *J Geophys Res* 2004;109(C18):3002–+. doi:10.1029/2003JC001962.
- 622 Woodgate RA, Aagaard K. Revising the Bering Strait freshwater flux into the Arctic Ocean.
623 *Geophys Res Let* 2005;32:2602–+. doi:10.1029/2004GL021747.
- 624 Woodgate RA, Aagaard K, Weingartner TJ. A year in the physical oceanography of the
625 Chukchi Sea: Moored measurements from autumn 1990–1991. *Deep Sea Research Part II:*
626 *Topical Studies in Oceanography* 2005;52:3116–49. doi:10.1016/j.dsr2.2005.10.016.